

A Physiologically Based Model of Discharge Pattern Regulation by Transient K^+ Currents in Cochlear Nucleus Pyramidal Cells

PATRICK O. KANOLD¹ AND PAUL B. MANIS²

¹The Center for Hearing Sciences and Department of Biomedical Engineering, The Johns Hopkins University School of Medicine, Baltimore, Maryland 21205; and ²Division of Otolaryngology-Head and Neck Surgery, Department of Surgery, University of North Carolina at Chapel Hill, Chapel Hill, North Carolina 27599-7070

Received 6 July 2000; accepted in final form 23 October 2000

Kanold, Patrick O. and Paul B. Manis. A physiologically based model of discharge pattern regulation by transient K^+ currents in cochlear nucleus pyramidal cells. *J Neurophysiol* 85: 523–538, 2001. Pyramidal cells in the dorsal cochlear nucleus (DCN) show three characteristic discharge patterns in response tones: pauser, buildup, and regular firing. Experimental evidence suggests that a rapidly inactivating K^+ -current (I_{KIF}) plays a critical role in generating these discharge patterns. To explore the role of I_{KIF} , we used a computational model based on the biophysical data. The model replicated the dependence of the discharge pattern on the magnitude and duration of hyperpolarizing prepulses, and I_{KIF} was necessary to convey this dependence. Phase-plane and perturbation analyses show that responses to depolarization are critically controlled by the amount of inactivation of I_{KIF} . Experimentally, half-inactivation voltage and kinetics of I_{KIF} show wide variability. Varying these parameters in the model revealed that half-inactivation voltage, and activation and inactivation rates, controls the voltage and time dependence of the model cell discharge. This suggests that pyramidal cells can adjust their sensitivity to different temporal patterns of inhibition and excitation by modulating the kinetics of I_{KIF} . Overall, I_{KIF} is a critical conductance controlling the excitability of DCN pyramidal cells.

INTRODUCTION

The set of intrinsic membrane conductances expressed by a neuron determines how different patterns of excitation and inhibition are transformed into output spike trains (Llinas 1988) or in other words, the signal processing operations that cells perform on the synaptically evoked voltage waveform. In the auditory system, many neurons show discharge patterns that appear to be closely regulated by cell-specific patterns of ion channel expression. Pyramidal cells of the dorsal cochlear nucleus (DCN) show a variety of different firing patterns to auditory stimulation in vivo (Godfrey et al. 1975; Pfeiffer 1966; Rhode et al. 1983). We demonstrated that the in vivo firing patterns could be replicated in vitro by varying the pattern of hyperpolarization and depolarization (Manis 1990). The discharge pattern changes were consistent with the increased activation of a transient (inactivating) A-type K^+ conductance (I_{KI}) (Connor and Stevens 1971) following a hyperpolarization (Manis 1990). Subsequent modeling studies with generic ionic conductances have supported this initial hypoth-

esis (Hewitt and Meddis 1995; Kim et al. 1994; Zhao 1993). Although these models represent a proof of principle and confirmation of the conceptual model, these models used arbitrarily defined cell and channel parameters and thus lacked a physiological basis.

Recently we characterized a fast transient potassium current (I_{KIF}) in vitro in identified DCN pyramidal cells (Kanold and Manis 1999b). The voltage and time dependence of conductance was well matched with the voltage and time dependence of the discharge patterns on prior membrane hyperpolarization, suggesting that I_{KIF} regulates the voltage-dependent discharge pattern in DCN pyramidal cells. A conclusive test of the role of I_{KIF} in generating the discharge patterns would be to remove the channel from the cell and observe whether the discharge patterns are altered. Unfortunately due to the diversity and sequence similarities of K^+ channels, few specific antagonists are available, and presently none are known to be specific for I_{KIF} .

Since we had characterized most outward currents present in DCN pyramidal cells on a detailed biophysical level (Kanold and Manis 1999b), this information was used to develop a computational model. Computational models have the advantage that conductances can be removed from the cell conveniently and the effects on the simulated discharge can be observed readily. In contrast to previously published models, the potassium channels in the model are based on in vitro data. The simulation results show that I_{KIF} is solely responsible for the observed voltage-dependent discharge patterns in DCN pyramidal cells. Moreover, we find that modifications of the voltage and time dependence of I_{KIF} alter the discharge patterns. The model is consistent with the experimentally observed range of voltage dependence and channel kinetics and suggests that these may be adjusted in individual cells to optimize processing of different patterns of afferent activity.

METHODS

Modeling was performed with programs implemented in C++ (Metrowerks Codewarrior 11) and executed as a MEX-file under MATLAB (version 5.2, The Mathworks, Natick, MA) on a Power Macintosh G3 (Apple, Cupertino, CA). Most results were also con-

Address for reprint requests: P. B. Manis, Div. of Otolaryngology-Head and Neck Surgery, Dept. Surgery, 610 Burnett-Womack Bldg., CB#7070, University of North Carolina at Chapel Hill, Chapel Hill, NC 27599-7070 (E-mail: pmanis@med.unc.edu).

The costs of publication of this article were defrayed in part by the payment of page charges. The article must therefore be hereby marked "advertisement" in accordance with 18 U.S.C. Section 1734 solely to indicate this fact.

firmed with the same equations implemented in NEURON, version 4.2 (Hines and Carnevale 1997).

The model pyramidal cell was represented by a single somatic compartment in which a membrane capacitance (C_m) is connected in parallel with voltage- and time-varying ionic conductances. While there is some evidence that the dendritic trees of DCN pyramidal cells contain active conductances (Manis and Molitor 1996; Molitor and Manis 1996), adding a passive dendritic tree or one with uniform active conductances did not quantitatively change the results shown here except for a decrease in the input resistance. Thus we performed all calculations on a point soma model.

The membrane contains five voltage-dependent ionic conductances and a leak conductance

$$-\frac{dV_m}{dt} = \frac{1}{C_m} * (I_{KIF}(V_m, t) + I_{KIS}(V_m, t) + I_{KNI}(V_m, t) + I_{Na}(V_m, t) + I_h(V_m, t) + I_L(V_m)) \quad (1)$$

Where I_{KIF} and I_{KIS} are the fast and slowly inactivating potassium currents, I_{KNI} is the noninactivating potassium current, I_h is the hyperpolarization-activated cation current, I_{Na} is the sodium current, and I_L is the leak current.

Kinetic descriptions

The currents were modeled as voltage- and time-dependent conductances using standard descriptions (Connor et al. 1977; Hodgkin and Huxley 1952) defined by time- and voltage-dependent activation and inactivation variables, termed the gating functions $x(V, t)$. The rate of change of the gating variables $x(V, t)$ are described by the first-order differential equation

$$\frac{dx(V, t)}{dt} = \frac{x_\infty(V, t) - x(V, t)}{\tau_x(V)} \quad (2)$$

Where $\tau_x(V)$ is the time constant and $x_\infty(V)$ is the steady-state value of $x(V, t)$. The activation variables are generically labeled m and the inactivation variables are labeled h .

Fast sodium current (I_{Na})

Because Na^+ currents have not been characterized in DCN pyramidal cells, a simple I_{Na} similar to other Na^+ channels in the literature in central neurons was implemented (Bernander et al. 1994). The kinetic equations for I_{Na} are given by

$$I_{Na}(V_m, t) = g_{Na} m_{Na}^2 h_{Na}(V_m - V_{Na}) \quad (3)$$

$$m_{Na\infty}(V_m) = (1 + e^{-[(V_m+38)/3]})^{-1} \quad (4)$$

$$h_{Na\infty}(V_m) = (1 + e^{(V_m+43)/3})^{-1} \quad (5)$$

The activation and inactivation time constants were treated as voltage independent and fixed at 0.05 and 0.5 ms, respectively. The maximal conductance, g_{Na} , was adjusted to 350 nS so that the action potential threshold and width were close to the physiological values. This description was chosen for convenience, and the exact form of the sodium conductance was not found to be critical to the modeling results presented here. Similar results were obtained using a temperature-scaled variation of the Hodgkin-Huxley sodium conductances (Hodgkin and Huxley 1952), and the state model of Moore and Cox (1976).

Inactivating potassium currents (I_{KIF} and I_{KIS})

The most prominent outward currents in the somata of DCN pyramidal cells are the fast and slow inactivating potassium currents I_{KIF} and I_{KIS} . The kinetic equations for I_{KIF} and I_{KIS} were directly derived

from the experimentally determined parameters (Kanold and Manis 1999b)

$$I_{KIF}(V_m, t) = g_{KIF} m_F^4 h_F (V_m - V_K) \quad (6)$$

$$m_{F\infty}(V_m) = (1 + e^{-[(V_m+53)/25.8]})^{-1} \quad (7)$$

$$h_{F\infty}(V_m) = (1 + e^{(V_m+89.6)/6.7})^{-1} \quad (8)$$

$$\tau_{mF}(V_m) = (0.15 * e^{(V_m+57)/10} + 0.3 * e^{-[(V_m+57)/10]})^{-1} + 0.5 \quad (9)$$

$$\tau_{hF}(V_m) = (0.015 * e^{(V_m+87)/20} + 0.03 * e^{-[(V_m+87)/20]})^{-1} + 10 \quad (10)$$

$$I_{KIS}(V_m, t) = g_{KIS} m_S^4 h_S (V_m - V_K) \quad (11)$$

$$m_{S\infty}(V_m) = (1 + e^{-[(V_m+40.9)/23.7]})^{-1} \quad (12)$$

$$h_{S\infty}(V_m) = (1 + e^{(V_m+38.4)/9})^{-1} \quad (13)$$

$$\tau_{mS}(V_m) = (0.15 * e^{(V_m+40)/10} + 0.3 * e^{-[(V_m+40)/10]})^{-1} + 0.5 \quad (14)$$

$$\tau_{hS}(V_m) = 200 \quad (15)$$

Since the average experimentally determined population time constants for activation and inactivation of the three K^+ currents showed little voltage dependence (Kanold and Manis 1999b), the activation time constants of I_{KIS} and I_{KIF} were initially fixed at 0.8 ms, and the inactivation time constants were fixed at 11 and 200 ms, respectively. Although the model reproduced the dependence of the discharge pattern on prepulse amplitude and duration, the model failed to reproduce the sharp transitions in firing patterns observed experimentally. In general, however, rate constants governing ion channel state transitions are voltage dependent. Re-examination of the data showed that currents from individual outside-out patches, and in whole cells, showed voltage-dependent activation and inactivation kinetics (i.e., see Kanold and Manis 1999b, Fig. 5). Hence, we incorporated voltage dependent time constants into this model. The activation time constants of I_{KI} in individual isolated cells obtained from the data shown in Kanold and Manis (1999b, Fig. 9) are shown in Fig. 1A (thin lines). The voltage dependence of the activation time constants of I_{KIF} and I_{KIS} (τ_{mF} and τ_{mS}) were modeled to approximate the experimentally observed time constants. The activation time constants of I_{KIF} and I_{KIS} are shown in Fig. 1A (thick lines) and given by Eqs. 9 and 14. Figure 1B shows the inactivation time constant of I_{KI} in individual isolated cells (thin lines). The inactivation time constant of I_{KIF} (τ_{hF}) was modeled to approximate the experimentally observed time constants. The inactivation time constant for I_{KIF} is shown in Fig. 1B (solid line) and given by Eq. 10. Since the inactivation time constant of I_{KIS} is relatively large, it was kept voltage invariant. Note that there is large variability in the time constants; the effects of this variability will be explored in the simulations.

Noninactivating potassium current (I_{KNI})

A third potassium current was experimentally observed in both acutely isolated cells and in patches. This current was a noninactivating, and behaved according to the following equations

$$I_{KNI}(V_m, t) = g_{KNI} m_N^2 (V_m - V_K) \quad (16)$$

$$m_{N\infty}(V_m) = (1 + e^{-[(V_m+40)/3]})^{-1} \quad (17)$$

As we did not have detailed data on the voltage dependence of activation time constant for this conductance, the activation time constant of I_{KNI} was treated as voltage independent and adjusted from the experimentally obtained values of 1–5 ms at 22°C to 0.5 ms (at our equivalent temperature of 32°C) to yield an action potential width of ~1 ms.

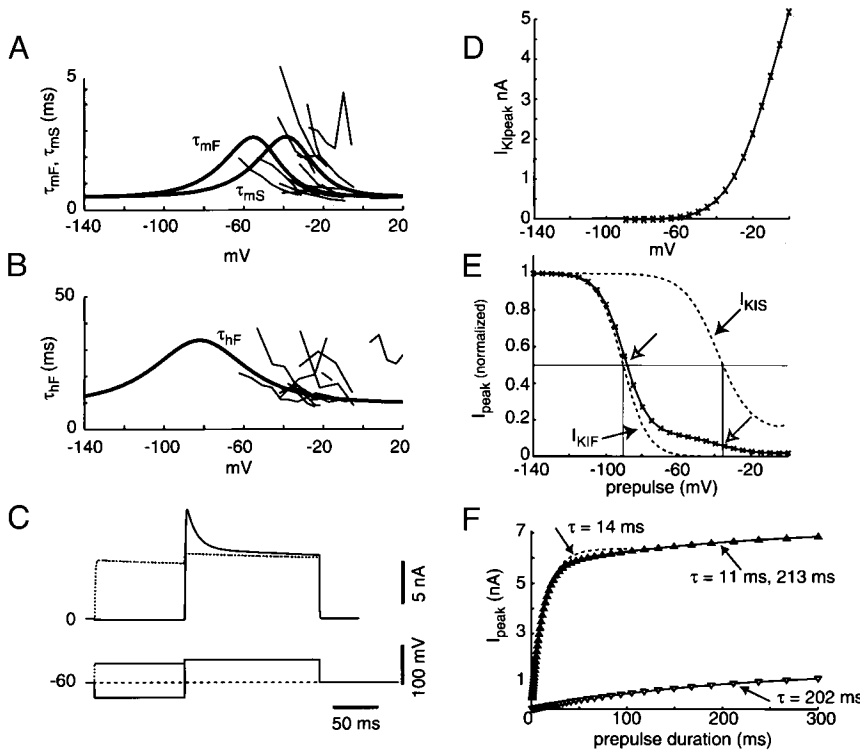


FIG. 1. *A* and *B*: voltage dependence of time constants of I_{KIF} and I_{KIS} . Thin lines indicate the experimentally determined time constants from individual isolated cells (fit assuming 4th-order activation). The thick lines indicate the time constants used in the model. *A*: activation time constants τ_{mF} and τ_{mS} of I_{KIF} and I_{KIS} . *B*: inactivation time constant τ_{hF} of I_{KIF} . *C*: example traces from model cell under voltage clamp. *Top*: depolarizing step to +10 mV with prepulses to -100 (solid) or 0 mV (dashed line). Note the rapidly inactivating transient current. *D*: activation curve for peak current in simulated voltage-clamp experiments with -100 mV prepulses as in *C*. Peak current near 0 mV is ~5 nA. *E*: inactivation curve of the peak transient current (solid line). The curve showed 2 points of inflection, suggesting double Boltzmann behavior. Arrows indicate estimated half-voltages of the 2 components. Dashed lines: blocking I_{KIS} or I_{KIF} yields the inactivation curves of remaining currents I_{KIF} and I_{KIS} , respectively. I_{KIF} has a half-inactivation at about -90 mV, whereas I_{KIS} shows half-inactivation at about -40 mV. *F*: summary of recovery from inactivation as function of prepulse length in simulated voltage-clamp experiments. Upright triangles: peak transient current. The data were best fitted with a double exponential with time constants of 11 and 213 ms (solid line). Dashed line is a fit with a single exponential with a time constant of 14 ms. Inverted triangles: recovery of the peak transient current with I_{KIF} set to 0. The data were best fitted with a single exponential with a time constant of 202 ms (solid line), corresponding to the recovery of I_{KIS} .

Hyperpolarization activated potassium current (I_h)

Pyramidal cells show a gradual decrease in hyperpolarization ("sag") during long hyperpolarizing pulses (see Kanold and Manis 1999b; Manis 1990). In addition, the membrane time constant is shorter for depolarizations after hyperpolarizations than for hyperpolarizing steps from the same voltage (Manis 1990; unpublished observations). One conductance that could produce these features is a nonselective hyperpolarization-activated cation current (I_h). Therefore a previously published description of I_h (Destexhe and Babloyantz 1993; Destexhe et al. 1993) was incorporated into the model. I_h activated below -40 mV and thus contributed slightly to the resting input resistance. Activation of I_h reduced the membrane time constant (measured in response to a depolarization at the end of a 100-ms hyperpolarizing step to -100 mV) τ_m from 3.2 to 2 ms. I_h is defined as

$$I_h(V_m, t) = g_h m_h n_h (V_m - V_h) \quad (18)$$

$$m_{hx}(V_m) = n_{hx}(V_m) = (1 + e^{(V_m + 68.9)/6.5})^{-1} \quad (19)$$

$$\tau_{mh}(V_m) = (1 + e^{(V_m + 183.6)/15.24})^{-1} \quad (20)$$

$$\tau_{nh}(V_m) = (1 + e^{(V_m + 158.6)/11.2}) * (1 + e^{(V_m + 75)/5.5})^{-1} \quad (21)$$

Leakage current (I_L)

The leakage current representing resistive losses over the membrane was described by Ohm's law

$$I_L(V_m) = g_l (V_m - V_l) \quad (22)$$

The leak conductance was adjusted so that the whole cell input resistance (R_m) at rest (-60 mV) was close to the experimental value of ~300 M Ω determined in isolated cells. The actual values were 284 M Ω in the MATLAB model and 300 M Ω in the NEURON model. The resting conductance of the cell is determined by the sum of all voltage-gated conductances and the leak current. The summed resting conductance of the voltage-gated channels (excluding the leak con-

ductance) was computed and the difference between this value, and the target input conductance of the cell was set as the leak conductance, which in this model was 2.8 nS. V_L was set to -57.7 mV to obtain a resting potential of -60 mV, similar to the resting potential of pyramidal cells in vitro (Hirsch and Oertel 1988; Kanold and Manis 1999b; Manis 1990; Zhang and Oertel 1994).

The reversal potentials for potassium (V_K) and sodium (V_{Na}) were adjusted to -81.5 mV (as measured from patches) and 50 mV (as estimated) respectively.

Scaling

In our experiments (Kanold and Manis 1999b), K⁺ channel kinetics were measured in outside-out patches. However, the exact geometry of the patch and hence its area was unknown, and it is likely based on our observations that the somatic distribution of channels is uneven. We therefore considered several factors in setting the magnitudes of conductances. First, the whole cell capacity C_m was chosen to match passive membrane properties of acutely isolated whole cells from rat DCN (Kanold and Manis 1999b). Isolated DCN cells in rat pup have narrow fusiform somas >20 μ m in length, with C_m ranging from 12 to 16 pF. These capacitance values are consistent with a spherical soma of ~20 μ m diam, assuming the standard membrane capacitance density of 1 μ F/cm² (Hille 1992). We choose the isolated cells as the target for these simulations because we had accurate measurements of whole cell currents and input resistances for this situation. In intact cells in slices, failure to adequately voltage-clamp dendritic membrane prevented us from obtaining acceptable estimates for the maximal conductances. The input resistance of the isolated cells averaged 300 M Ω , whereas the input resistances of outside-out patches varied from 3 to 8 G Ω . Using a scale factor of 30 (~8G Ω /300M Ω), we obtained total outward currents at 0 mV of ~5 nA, consistent with our whole cell voltage-clamp data (Fig. 1D). In additional simulations (not shown), we adjusted this scale factor to mimic an intact cell. The cell capacitance and all conductances were raised again by a factor of ~20 (to set C_m to 250 pF, consistent with $R_{in} = 50$ M Ω and $\tau_m = 12$ ms), and the input resistance adjusted via the leak conductance to

50 M Ω . Although larger currents were required to obtain equivalent voltage displacements due to the lower input resistance, the results were the same.

The relative conductance ratios of the different outward currents were derived from the experimental measurements. The conductance of I_{KIF} (g_{KIF}) in patches varied from 1.5 to 14 nS and averaged ~ 5 nS; thus after scaling from patch to whole cell, g_{KIF} was set to 150 nS. The measured amplitude of I_{KIS} in patches is about one-fourth the amplitude of I_{KIF} (see Kanold and Manis 1999b, Fig. 3), so g_{KIS} was set to 40 nS. The maximum conductance of g_{KNI} as scaled from patches to whole cell would be 20 nS. However, this value was too small to rapidly repolarize action potentials and produce action potentials followed by undershoots. Setting g_{KNI} to 80 nS yielded appropriate action potential shapes and physiological action potential height. We justify this difference on the grounds that channel densities may be higher in the initial segment of the axon where action potentials are most likely initiated (Colbert and Johnston 1996; Stuart et al. 1997), whereas our estimates were from conductances sampled from the soma.

The magnitude of I_h (g_h) was determined from estimates of the equivalent parallel conductance generated by the sag during the hyperpolarizing prepulse in current-clamp recordings from slices, which was 34 nS. This value was then scaled by the relative capacitance of the isolated cells versus the equivalent capacitance determined from the τ_m of cells in slices, yielding a whole cell conductance for g_h of 3 nS. V_h was set to -43 mV (Destexhe and Babloyantz 1993; Destexhe et al. 1993). The magnitude and time course of the sag produced by this conductance closely resembled that seen in intracellular recordings from DCN pyramidal cells.

Voltage-clamp simulations

To confirm the behavior of the model, we compared the size and voltage dependence of the currents with the experimentally obtained voltage-clamp data from acutely isolated cells and outside-out membrane patches. In these voltage-clamp simulations, g_{Na} is set to zero to eliminate the contribution of Na^+ channels. Activation of the transient currents was studied using a prepulse protocol similar to the protocol used experimentally, in which the membrane was held either at 0 or -100 mV to inactivate or deinactivate both transient currents, respectively. The prepulse was followed by a test step to a varying voltage. The transient current was inactivated by depolarizing prepulses (Fig. 1C), and was activated near the resting potential of -60 mV (Fig. 1D). The size of the transient current, its kinetics, and its activation voltage is in the range of the experimental results for acutely isolated cell bodies (Kanold and Manis 1999b). Steady-state inactivation was measured by preceding a depolarizing step with a prepulse to various voltages (Fig. 1C). The current showed a pronounced transient component after hyperpolarizing prepulses; the amplitude of the transient current was smaller following depolarizing prepulses. Figure 1E shows the normalized peak transient current as function of prepulse voltage. Similar to the experimental data (Kanold and Manis 1999b, Fig. 4), the inactivation shows a double Boltzmann shape with half voltages of about -90 and about -40 mV (arrows indicate the estimated midpoints of the 2 inflections). Setting either g_{KIS} or g_{KIF} to zero resulted in single Boltzmann curves (Fig. 1E, dashed lines) that correspond to the inactivation curves of the unblocked current. Eliminating I_{KIF} resulted in a single Boltzmann curve (long dashed line) with a half inactivation of about -40 mV (vertical thin line), which corresponds to the half inactivation of I_{KIS} . When I_{KIS} was removed, a single Boltzmann curve (short dashed line) was observed with a half inactivation of about -90 mV (vertical thin line), which corresponding to half-inactivation of I_{KIF} . These results are similar to those seen with pharmacological block of I_{KIS} (see Kanold and Manis 1999b, Fig. 6). When I_{KIS} was blocked by TEA or 4-aminopyridine (4-AP), the blocked current (determined by subtraction) had half-inactivation at about -40 mV. I_{KIF} was TEA and 4-AP resistant and showed

half-inactivation at about -90 mV. The double Boltzmann shape in the model is not as pronounced as in some of the experimental data (i.e., see Kanold and Manis 1999b, Fig. 6), probably reflecting varying ratios of I_{KIF} and I_{KIS} in outside-out patches. These results show that the activation and inactivation of the potassium currents in the model is similar to the experimental observations.

We also measured the recovery of I_{KI} from inactivation while varying the length of the hyperpolarizing prepulse. The amplitude of the transient current was maximal after long hyperpolarizing steps, whereas it was reduced after short steps. When the time course of recovery of the peak current (Fig. 1F, upright triangles) was fitted with a single exponential function over the range of prepulse durations studied experimentally, the resulting time constant was 14 ms (Fig. 1F, dashed line). This time constant is similar to the experimentally observed time constants. We previously found that the recovery of I_{KI} was slightly longer than the dependence of the first spike latency shift on prepulse duration (time constants of 15–20 vs. 10 ms) (Kanold and Manis 1999b). In the model, it was apparent that the recovery time course of I_{KI} was better described with a double exponential function, with a fast and a slow time constants of 11 and 213 ms (Fig. 1F, solid line), suggesting that removal of inactivation for the two currents (I_{KIF} and I_{KIS}) proceeds with different time courses. Removing I_{KIF} from the model resulted in smaller outward transient current and the residual recovery time course was best fit with a single exponential function with a time constant of 202 ms (Fig. 1F, inverted triangles and solid line), corresponding to the time course of removal of inactivation for I_{KIS} . These results indicate that the behavior of the transient currents in the model closely parallels that of the experimentally studied potassium currents.

RESULTS

The behavior of the point soma model of a DCN pyramidal cell in a variety of experimental conditions will be investigated and compared with the experimental observations reported previously (Kanold and Manis 1999b). The results are presented in two parts. First, current-clamp simulations will be presented and we show that the discharge patterns match the experimental observations. Second, we show how modifications of I_{KIF} voltage dependence and kinetics within the experimentally observed range alter the dependence of the discharge pattern on prepulse amplitude and duration.

Spike rate

First, the response of the model to current pulses of varying amplitudes from rest was examined. The model did not spontaneously fire action potentials at rest. Depolarizing current injections produced trains of action potentials (Fig. 2A). The sustained discharge was very regular, similar to results obtained in vitro (Hirsch and Oertel 1988; Kanold and Manis 1999b; Manis 1990; Zhang and Oertel 1994). The spike frequency increased monotonically and showed some saturation for large injection currents (Fig. 2B). For small currents, the firing rate increased with a slope of 1,012 Hz/nA. This slope is about nine times higher than experimentally measured in slices from guinea pig (116 Hz/nA) (Manis 1990), three to nine times higher than in mice (100–300 Hz/nA) (Zhang and Oertel 1994), and four times higher than that in gerbil (258 Hz at 1 nA) (Ding et al. 1999). The difference in slopes can be explained by the higher input resistance of the somatic model as compared with a cell in slices (300 vs. ~ 30 M Ω). Larger model cells with dendritic compartments or single compartment models with lower input resistances showed spike rates

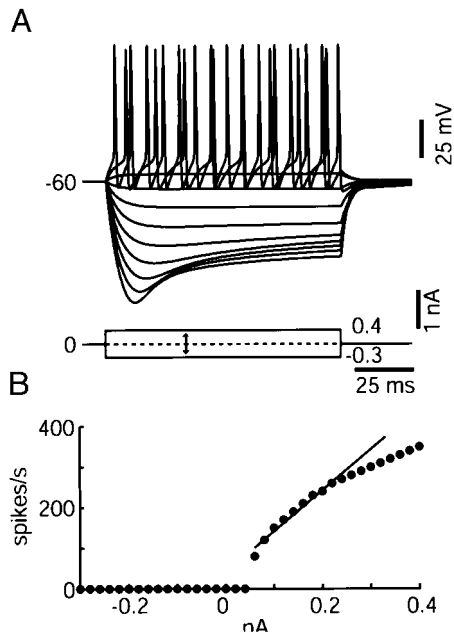


FIG. 2. Firing rate as a function of injection current. *A*: injection of long-lasting depolarizing (100 ms) currents from -300 to 400 pA resulted in trains of action potentials. *B*: spike rate as a function of current amplitude. Spike threshold is 50 pA. The spike rate increased monotonically with a slope of $1,012$ spikes \cdot nA⁻¹ \cdot s⁻¹ (regression line) before showing a sloping saturation.

similar to those in real cells (not shown). For hyperpolarizing current injections, a “sag” was present in the response, reflecting activation of I_h , which is similar to experimental results (Manis 1990).

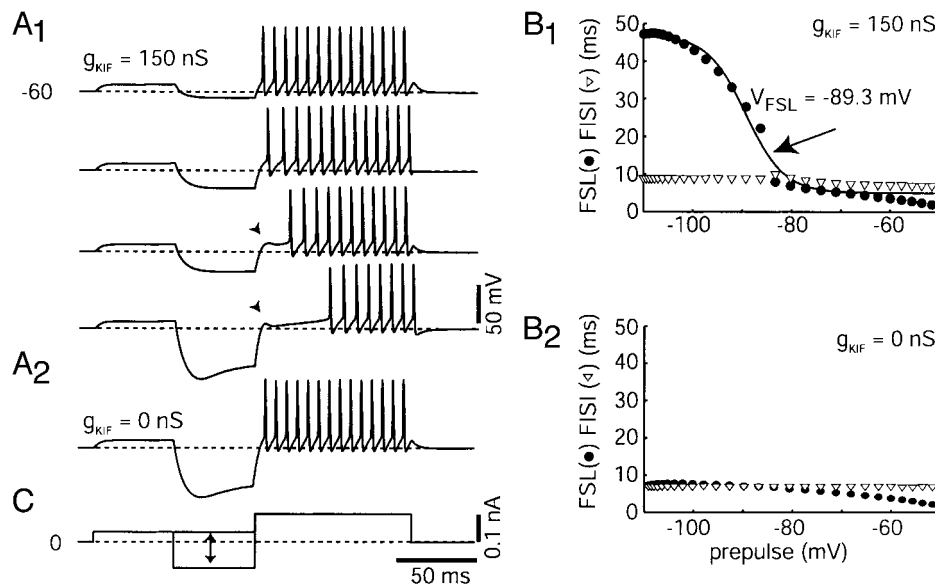


FIG. 3. Voltage dependence of 1st spike latency (FSL) and 1st interspike interval (FISI). *A1*: responses to a constant depolarizing current step after a 50-ms hyperpolarization to different levels (-68.0 , -83.3 , -86.3 , -109.0 mV). The dashed line in each trace indicates the resting potential of -60 mV. The hyperpolarizing pulses were preceded by a depolarizing step below spike threshold to inactivate transient K⁺ currents. Arrow points to “hump and sag” response. Note the sharp increase in FSL between the 2nd and 3rd traces, corresponding to the elimination of the onset spike. *A2*: removal of I_{KIF} from the model eliminates the long FSL after hyperpolarizing steps. *B1*: latency and FISI as a function of prepulse voltage. The FSL (filled circles) increases with increasing hyperpolarization between -60 and -100 mV, whereas the FISI (open triangles) is nearly constant. The solid line indicates a Boltzmann fit with a half-voltage (V_{FSL}) of -89.3 mV. The arrow points to the sharp transition in firing pattern. *B2*: when I_{KIF} is removed, the increase of the FSL with increasing hyperpolarization is less pronounced. The FISI is unchanged from the control conditions. *C*: the current injection protocol for *A*.

Dependence of the discharge pattern on prepulse voltage

Next, we investigated how the first spike latency (FSL) and first interspike interval (FISI) depend on the prepulse voltage. In pyramidal cells, the FSL and FISI are a function of the depth and duration of hyperpolarization preceding a test depolarization (Kanold and Manis 1999b; Manis 1990). In these simulations, we used a 50-ms subthreshold depolarization to partially inactivate transient currents, as we did experimentally. This was done to help insure that the state of the channels at the start of the hyperpolarizing pulse was the same in all cells. The traces in Fig. 3*A1* demonstrate the effect of varying the prepulse amplitudes. For small hyperpolarizations, there was little change in latency. However, as the hyperpolarization was increased further, the latency suddenly increased. When the latency increased, there was a characteristic “hump and sag” of the membrane potential at the onset (arrowheads in Fig. 3*A1*). In Fig. 3*B1* the FSL (circles) and FISI (triangles) are plotted as a function of prepulse voltage. Most of the FSL increases occur when the prepulse voltage is between -80 and -110 mV. The largest increase in FSL occurred between -86.3 and -83.3 mV (arrow in Fig. 3*B1*); this corresponds to the disappearance of the onset spike (arrowhead in Fig. 3*A1*). The increase in FSL at this point is similar to the duration of the FISI, so that the first spike now occurs approximately where the second spike occurs without prior hyperpolarization. To estimate the half-voltage for the FSL shift, a Boltzmann function was fitted to the data (Fig. 3*B1*, solid line). The half voltage was -89.3 mV, which is similar to values obtained experimentally using the same analysis (Kanold and Manis 1999b).

To test the hypothesis that the voltage-dependent FSL shift is due to I_{KIF} , g_{KIF} was set to zero as shown in Fig. 3*A2* for the

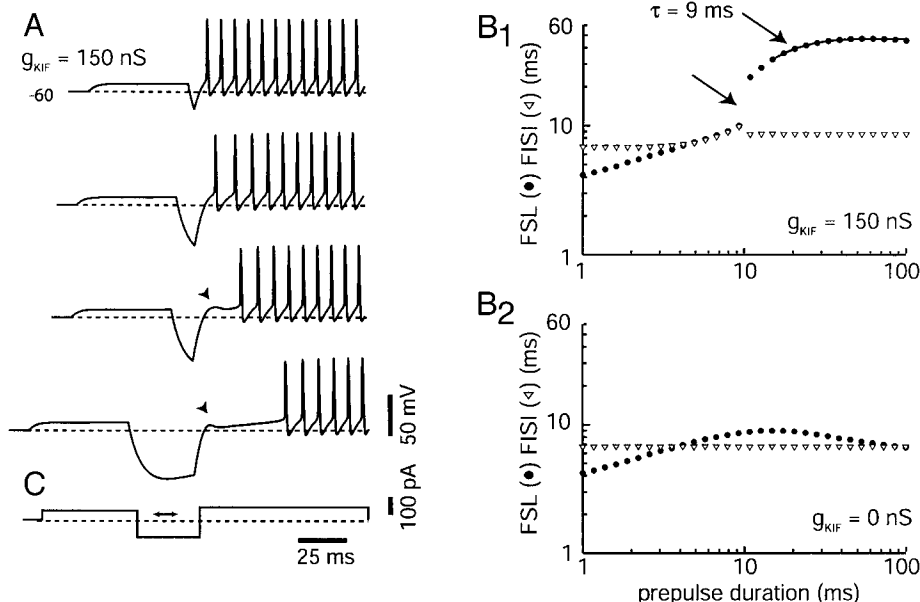


FIG. 4. Time dependence of FSL and FISI. A: responses to a depolarizing current step following hyperpolarizing pulses of varied duration (3.0, 9.2, 10.8, 32.9 ms). Note the development of the long FSL response and the sharp firing pattern transition. The current injection protocol is shown in C. B1: FSL as function of prepulse duration. FSL (filled circles) increases approximately linearly with pulse duration until ~ 10 ms, at which the FSL increased rapidly (arrow). The increase in FSL after this time point could be approximated by a single exponential with a time constant of 9 ms (solid line). B2: removal of I_{KIF} decreases the increase in FSL after longer hyperpolarizing steps.

most hyperpolarized prepulse voltage. The FSL was slightly longer than with no prepulse, probably because of the increased passive charging time of the membrane. The shift in FSL with increasing hyperpolarization is small, as shown in Fig. 3B2. These results show that I_{KIF} is necessary for the generation of voltage-dependent discharge patterns.

Dependence of the discharge pattern on prepulse duration

We next examined the effect of changing the duration of the hyperpolarizing prepulse on the FSL. Figure 4A shows four traces with varying prepulse durations. Increasing the length of the prepulse from 3.0 to 9.2 ms increased the FSL from 6.2 to 10.0 ms. However, lengthening the prepulse further to 10.8 ms increased the FSL to 23.7 ms. Note that the first spike occurs at a latency just slightly longer than the second spike for a prepulse duration of 9.2 ms, indicating that the onset spike has been deleted (arrowhead). The voltage showed a hump and sag in place of the deleted onset spike. The cell fires now with a buildup pattern. Further increases in the prepulse duration lead to a further increase in FSL. The FSL increased linearly for short prepulses (Fig. 4B1), probably due to passive charging of the membrane, and then abruptly transitioned to a long FSL pattern. Note the small concurrent changes in FISI at the transition point (open triangles).

The shift in FSL with prepulse duration was fitted with a single exponential function (Fig. 4B1, solid line), with a time constant of 9 ms, similar to that seen experimentally (Kanold and Manis 1999b). Removal of I_{KIF} abolished most of the dependence of the FSL on the prepulse duration (Fig. 4B2, filled circles). A small residual linear FSL shift was present after the removal of I_{KIF} for short prepulses. This shift is also seen with I_{KIF} (Fig. 4B1) and is probably due to passive charging of the membrane. The FSL decreases for long hyperpolarizing steps, an effect likely due to the activation of I_h , which lowers the membrane time constant during repolarization. These results suggest that increased availability of I_{KIF} is directly responsible for the increase in FSL with longer hyperpolarizing

steps. They also suggest that I_h may play a modulatory role in this process.

Transitions between discharge patterns

To this point, it has been demonstrated that the model showed a regular or buildup pattern after hyperpolarizing prepulses, depending on the prepulse amplitude. Pyramidal cells can show a regular, buildup, or pauser pattern or transition between these patterns depending on the levels of hyperpolarization and depolarization (see Kanold and Manis 1999b; Manis 1990). The transition from a buildup to a pauser pattern usually occurs when the depolarization is made larger.

Figure 5 shows the response of the model to several prepulse levels while testing with larger depolarizing currents (200 instead of 100 pA). Now the model responds with an increased FISI, but a short FSL, following hyperpolarized pulses (Fig. 5A1, \downarrow). This is the hallmark of the pauser pattern. The increase in FISI largely occurs between -80 and -110 mV, with an estimated half voltage of -99 mV (Fig. 5B), similar to the range observed in vitro (Kanold and Manis 1999b). Pauser responses were abolished when I_{KIF} was removed from the model (not shown). The model also changed firing pattern from regular to pauser as the length of the hyperpolarizing pulse was increased (Fig. 5, C and D); however, the transition in this case is more gradual than that shown in Fig. 4.

Intermediate amplitude (150 pA) depolarizing steps caused the model to show all three discharge patterns when varying the prepulse hyperpolarization (Fig. 6, A and C). For small hyperpolarizations, the model showed a regular discharge pattern, whereas increasing the amount of hyperpolarization caused a switch to a pauser pattern (arrow in Fig. 6A1). With further hyperpolarization, the onset spike failed (arrowhead) and the model fired with a buildup pattern. The transition between pauser and buildup pattern is visible as a large increase in FSL and an associated decrease in FISI (Fig. 6B). Similar transitions between firing patterns were seen in vitro (Kanold and Manis 1999b; Manis 1990). The model also changed firing pattern from regular to pauser to buildup as the

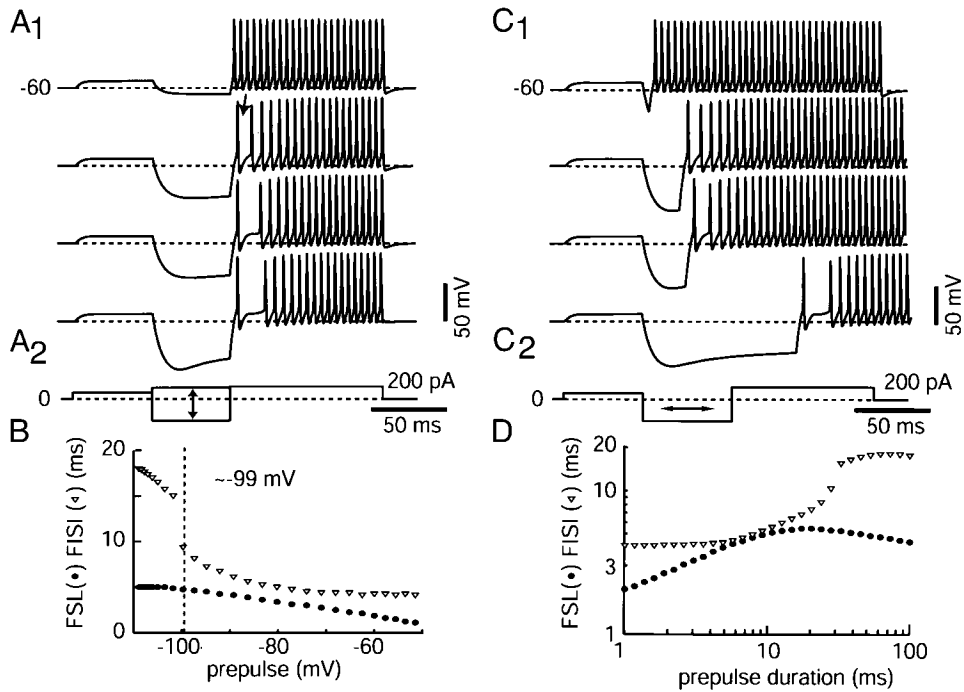


FIG. 5. Pauser responses. *A1*: responses to different prepulse amplitudes with a depolarization to 200 pA (current protocol shown in *A2*). Note the development of a long FISI (\downarrow) for hyperpolarized steps. *B*: the FISI (∇) increases with increasing hyperpolarization between -80 and -110 mV. \downarrow , the half voltage. *C1*: responses to varied prepulse duration (shown in *C2*). The model developed a long FISI. *D*: FSL and FISI as function of prepulse duration. The FISI increases with prepulse duration, then saturates.

length of the hyperpolarizing pulse was increased (Fig. 6, *C* and *D*).

To summarize, the model can show all three discharge patterns: regular, buildup, and pauser. Which pattern is produced depends on the levels of prehyperpolarization and on the magnitude of the test depolarization. The voltage and time dependence of these patterns is similar to that seen in cells in brain slices, including the sharp transitions between firing modes that are seen with small changes in stimulation conditions. It appears that I_{KIF} controls these discharge patterns since when it is removed from the model, the cell only fires regularly regardless of the stimulus conditions.

Influence of the half-inactivation voltage of I_{KIF} on discharge pattern

If I_{KIF} controls the discharge patterns of the cells, then the voltage dependence of the FSL and the inactivation of I_{KIF} should be related. Indeed, a wide range of half-inactivation voltages of I_{KIF} (V_{KIF}) and half-voltages of the FSL shift (V_{FSL}) were observed experimentally (Kanold and Manis 1999b). To directly test this hypothesis, V_{KIF} was varied from its control value of -89.6 mV to values ranging from -99.6 to -64.6 mV. Figure 7*A* shows the results of parametric simulations in which both the prepulse amplitude and V_{KIF} were varied. The

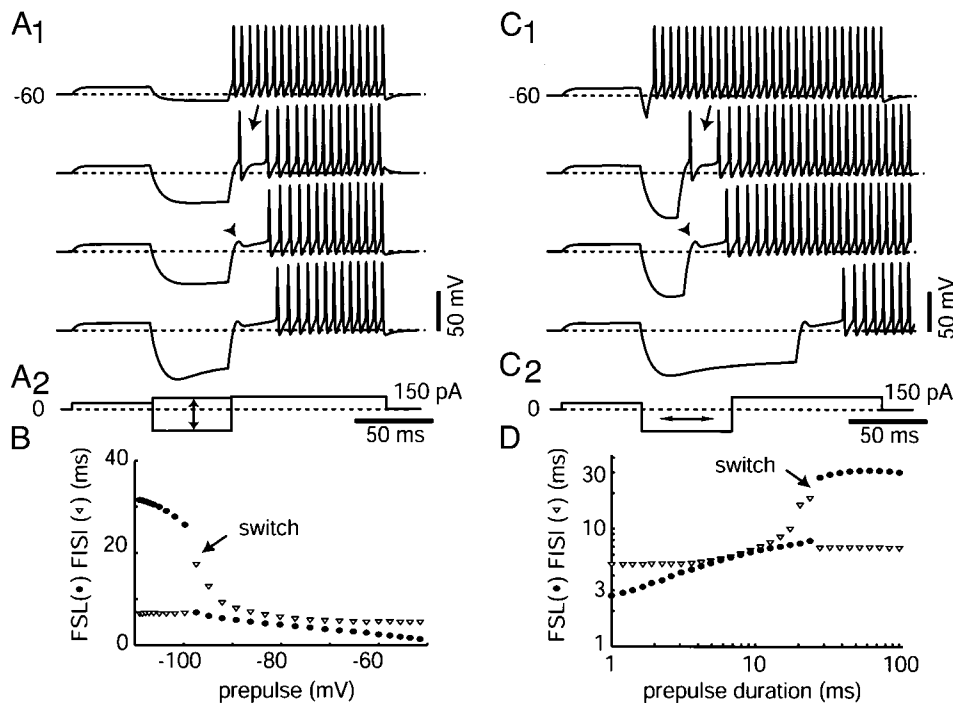


FIG. 6. *A1*: responses to different prepulse amplitudes with a depolarization to 150 pA (current protocol shown in *A2*). Note the development of the long FISI (arrow) and switch to long FSL (arrowhead) for hyperpolarized steps. *B*: the FSL (filled circles) and FISI (unfilled triangles) at different prepulse levels. The FISI increases gradually with hyperpolarization between -80 and -100 mV, and then abruptly decreases as the FSL increases. *C1*: responses to different prepulse durations (shown in *C2*). The model developed a long FISI and then switched to a long FSL. *D*: FSL and FISI as function of prepulse duration. Note the sharp transition in firing pattern (arrow) for a prepulse duration of 25 ms.

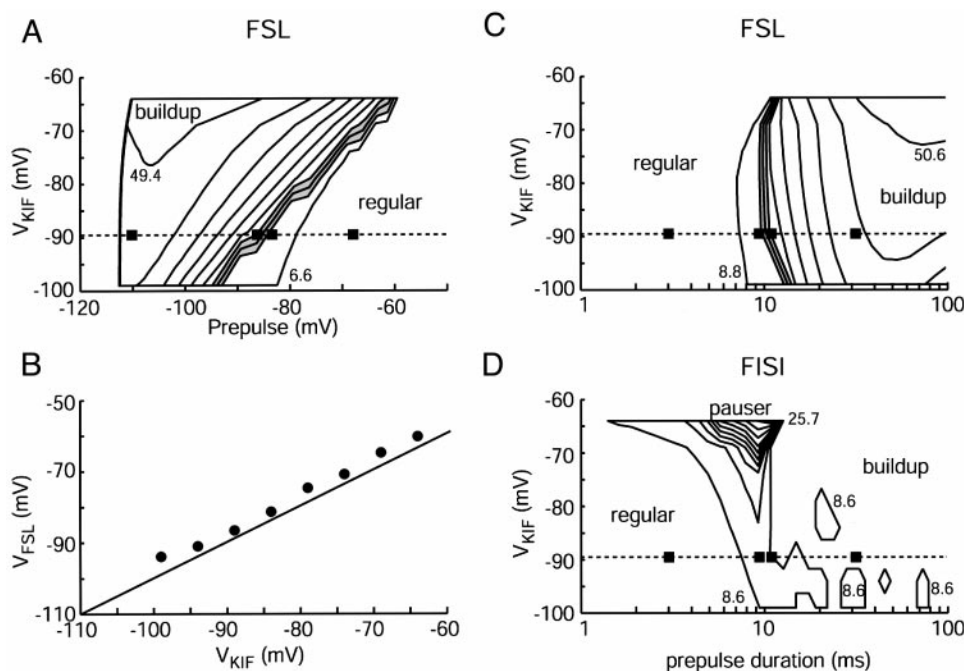


FIG. 7. Relationship of the half-inactivation voltage of I_{KIF} and the voltage and prepulse duration dependence of the discharge pattern. The half-inactivation voltage of I_{KIF} (V_{KIF}) was varied from the control value of -89.6 mV between -99.6 and -64.6 mV. The amplitudes of the depolarizing current injection (100 pA) were identical for each value of V_{KIF} . *A*: contour plot of the FSL as function of prepulse voltage for different values of V_{KIF} using the protocol shown in Fig. 3C. ---, the control condition. ■, correspond to the traces shown in Fig. 3A1. FSL contours range from 6.6 to 49.4 ms and are spaced at ~ 5 ms. Shaded region shows area of steepest transition. As V_{KIF} is increased the transition from short to long FSL shifts toward less hyperpolarized prepulse voltages. *B*: the half-voltage of Boltzmann functions fit to the data (V_{FSL}) is linearly related to the half-inactivation voltage of I_{KIF} (V_{KIF}). —, unit slope. *C*: contour plot of the FSL as function of prepulse duration for different values of V_{KIF} using the protocol shown in Fig. 4C. ---, the control condition. ■, the condition of traces shown in Fig. 4A1. The FSL contours ranged from 8.8 to 50.6 ms and are spaced at ~ 5 ms. Shaded region shows area of steepest transition. The duration at which the response transitions to a buildup pattern is only slightly dependent on V_{KIF} . *D*: contour plot of the FISl as a function of prepulse duration for different values of V_{KIF} . Contours ranged from 8.6 to 25.7 ms are spaced at ~ 2 ms. Note the emergence of pauser responses for prepulses between ~ 4 and ~ 12 ms when V_{KIF} is close to the resting potential.

plot shows contour lines of the FSL during these trials; regions associated with particular discharge modes are indicated on the graph. For small hyperpolarizations and negative V_{KIF} , no increase in FSL is seen; the cell always fires in a regular pattern. However, increasing the hyperpolarization to near -100 mV results in a large increase in FSL, corresponding to the buildup pattern. When V_{KIF} is made more positive, then the region of rapid FSL increase occurred at less hyperpolarized prepulse levels. For example, when V_{KIF} is -64.6 mV, the cell fires with a buildup response for prepulses just below the resting potential. For these conditions (100 -pA depolarizing test pulse), the FISl shows little change for any combination of prepulse voltage. To explore the association between half-inactivation and FSL voltage dependence, the half-voltage of the Boltzmann fit to the prepulse voltage dependence for each value of V_{KIF} was computed as shown in Fig. 3B1. These data almost fell on a line with a slope of 1 (Fig. 7B, —), suggesting that the region of the main latency shift and the half-inactivation voltage of I_{KIF} are strongly correlated. We also analyzed the model using 200 -pA depolarizations, where cells show a transition from regular to pausing patterns. The results were similar in that the FISl was strongly correlated with V_{KIF} (not shown).

Next we investigated how variations of the half-inactivation voltage of I_{KIF} (V_{KIF}) affect the dependence of the FSL on prepulse duration. Figure 7, C and D, shows the dependence of

FSL and FISl on prepulse duration over a range of V_{KIF} . For a given combination of hyperpolarization and depolarization, the FSL is somewhat independent of V_{KIF} , except for long pulses where the latency shift depends on both pulse duration and V_{KIF} (Fig. 7C). In the same simulations, the FISl increased significantly when V_{KIF} was less negative for prepulse durations where a short FISl was produced under control conditions (Fig. 7D). For example, varying the prepulse duration with $V_{KIF} = -64.5$ mV yields a regular response for very short prepulses, pauser responses for prepulses between 4 and ~ 12 ms, and buildup responses for longer prepulses. Thus the prepulse duration necessary to initiate the transition from regular to pauser, and from pauser to buildup, depends on the value of V_{KIF} .

These simulations suggest that cells with different half-inactivation voltages for I_{KIF} will respond with different discharge patterns to the same stimulus. We suggest that the variability of the voltage dependence of the discharge patterns seen experimentally reflects the underlying variability of V_{KIF} . Moreover, if a cell can adjust V_{KIF} , then it can dynamically alter its response to a particular stimulus.

Influence of the kinetics of I_{KIF} on discharge pattern

Because voltage dependence of the FSL and the inactivation of I_{KIF} were related, we investigated how the kinetics of I_{KIF}

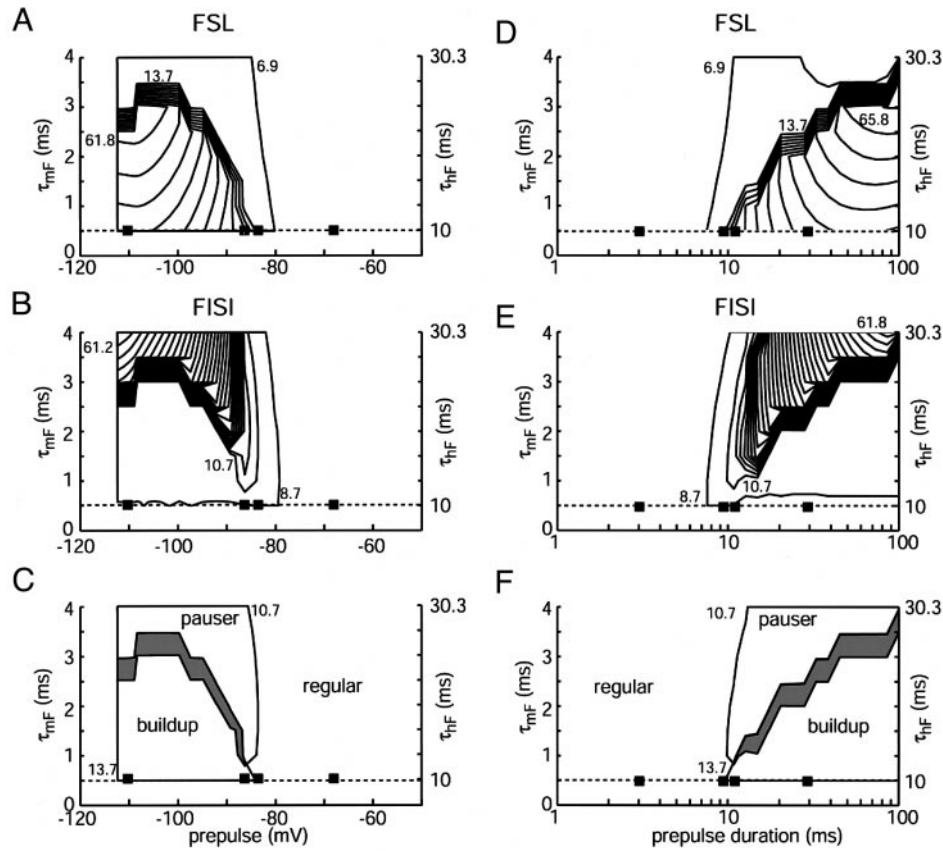


FIG. 8. Influence of the kinetics of I_{KIF} and the voltage and prepulse duration dependence of the discharge pattern. The base value of the activation time constant of I_{KIF} (τ_{mF}) was varied from the control value of 0.5 ms up to 4 ms. The base value of the inactivation time constant (τ_{hF}) was co-varied from 10 ms up to 30.3 ms. The amplitudes of the depolarizing current injection (100 pA) were identical for each value of τ_{mF}/τ_{hF} . A–C: effect of changes in prepulse voltage for different values of the time constants using the protocol shown in Fig. 3C. ---, the control condition. ■, the traces shown in Fig. 3A. A: contour plot of the FSL with contours ranging from 6.9 to 61.8 ms and spaced at ~ 5 ms. The transition from short to long FSL is shifted toward positive prepulse amplitudes as τ_{mF}/τ_{hF} are increased. The buildup region is bounded below the 13.7 ms contour. B: contour plot of the FISI with contours range from 8.7 to 61.2 ms and spaced at ~ 2 ms. Note the increase in FISI for hyperpolarized prepulses and larger values of τ_{mF} . The pauser region is circumscribed by the 10.7 ms contour. C: superposition of the FSL and FISI contours circumscribing the buildup and pauser regions, respectively. The overlap between the contours is shaded and indicates the transition zone between the pauser and buildup response areas. The response of the cell to prepulses of varying amplitude falls in 1 of the 3 regions depending on τ_{mF}/τ_{hF} . D–F: changes in prepulse duration for different values of the time constants. The effect of changing the prepulse amplitude was tested using the protocol shown in Fig. 4C. ---, the control condition. ■, the traces shown in Fig. 4A. D: contour plot of the FSL with contours ranging from 6.9 to 65.8 ms and spaced at ~ 5 ms. The transition to a long FSL pattern is shifted toward longer prepulse durations as τ_{mF}/τ_{hF} are increased. The buildup region is circumscribed by the 13.7 ms contour. E: contour plot of the FISI with contours ranging from 8.7 to 61.8 ms and spaced at ~ 2 ms. The FISI is increased for longer prepulses and larger values of τ_{mF}/τ_{hF} . The pauser region is circumscribed by the 10.7-ms contour. F: superposition of the FSL and FISI contours circumscribing the buildup and pauser regions, respectively. The overlap between the contours is shaded and indicates the transition zone between the pauser and buildup response areas. The response of the cell to prepulses of varying amplitude falls in 1 of the 3 regions depending on τ_{mF}/τ_{hF} . Note that increasing τ_{mF}/τ_{hF} shifts the transition point between pauser and buildup pattern monotonically.

influence the discharge pattern. The kinetics of I_{KIF} vary over a wide range (Kanold and Manis 1999b), and activation and inactivation rates appear to be correlated for individual cells. Therefore in the next set of simulations, we varied the base value of the activation time constant (τ_{mF}) from its control value of 0.5 ms to values up to 4 ms (this corresponds to a simple additive shift of the τ -V curves). To maintain the experimentally observed correlation between τ_{act} and the inactivation time constant (τ_{hF}), we also changed the base value of τ_{hF} according to the formula $\tau_{hF} = 7.1 + 5.8 * \tau_{mF}$ (Kanold and Manis 1999b). Figure 8, A and B, shows the effect of changing the kinetics of I_{KIF} on the FSL and FISI as the prepulse amplitude was varied. The parameters corresponding to the traces shown in Fig. 5A1 are indicated (--- and ■). Increasing

τ_{mF} and τ_{hF} caused an increase in the FSL shift for large hyperpolarizations (Fig. 8A). However, for intermediate hyperpolarizations between about -85 and -90 mV, large increases in FISI were seen when the time constants were increased (Fig. 8B). Thus the cell now responded in a pauser pattern instead of a buildup pattern. The plots of FSL and FISI are complimentary, indicating that there are discrete transitions between firing patterns for specific prepulse conditions, as τ_{mF}/τ_{hF} are varied. When we superimpose the contours that defined the borders of the increased FSL or increased FISI pattern (Fig. 8C), the resulting responses of the cell showed three discrete areas. First, there is an area where both FSL and FISI are short (labeled “regular”). Second, there is an area where FSL is long and FISI is short (labeled “buildup”). Finally, there is an area

where FISl is long and the FSL is short (labeled “pauser”). The shaded region indicates the transition zone between the pauser and buildup firing patterns. The prepulse voltages for this transition zone are directly related (but not completely monotonically) to the time constants of activation and inactivation. In general, increasing the time constants caused a shift of the pauser/buildup transition to more hyperpolarized potentials.

Varying the kinetics of I_{KIF} had a similar effect on the discharge pattern changes induced by varying prepulse duration (Fig. 8, *D* and *E*). Again, the regions of pauser and buildup responses are complementary. When τ_{mF} and τ_{hF} are increased, the cell fires with a pauser pattern for prepulse durations that generate a buildup pattern under control conditions (Fig. 8*F*). The prepulse duration at which the pauser/buildup transition occurred increases monotonically as τ_{mF} and τ_{hF} are increased.

These results show that the cells firing pattern to prepulses of particular amplitude or duration depends on the time constants of activation and inactivation of I_{KIF} . In conjunction with the results of the previous section, it appears that cells have two independent mechanisms by which they can control their firing patterns: adjustment of V_{KIF} or of the rates τ_{mF} and τ_{hF} .

Phaseplane analysis

The results presented in the preceding text strongly suggest that the availability of I_{KIF} , as controlled by its inactivation gating variable (h_F), is the crucial variable controlling the discharge pattern. To evaluate the association between the inactivation of I_{KIF} and the discharge pattern, especially around the transition between regular and buildup patterns, a phaseplane analysis was performed using the model under standard conditions of V_{KIF} and τ_{mF}/τ_{hF} . Figure 9*A1* shows the voltage traces used for the analysis. The thin trace was obtained with a hyperpolarizing prepulse of 9.2 ms (generating a regular discharge pattern), and the thick trace was obtained with a 10.8-ms prepulse (generating a buildup discharge pattern). The

traces have been aligned at the onset of the test depolarization. Figure 9*A2* shows the time course of the inactivation gating parameter of I_{KIF} (h_F). During the 9.2-ms hyperpolarizing pulse, h_F increases from its steady-state value at rest of 0.012 to 0.164 at the onset of depolarization (thin line). A prepulse of 10.8 ms resulted in an increase of h_F to 0.225 at the onset of depolarization (thick line). As the cell was depolarized, h_F increased to a maximum of 0.203 and 0.266, respectively. These results suggested that a critical amount of I_{KIF} had to be deinactivated to cause discharge pattern transitions and that this amount was between 16.4 and 22.5% of the maximal I_{KIF} .

The trajectory of h_F during the voltage excursion is presented with phaseplane plots during the hyperpolarization, the rising phase of the membrane voltage, and the first few spikes in Fig. 9*B1*. h_F increased during the hyperpolarization. The transition between the two discharge patterns is visible as a divergence in the trajectory (arrow) between the 9.2 ms (thin line) and 10.8 ms (thick line) condition. For the same traces, the activation of I_{KIF} (m_F) showed a much smaller dependence on prepulse duration (Fig. 9*B2*).

To test whether the amount of inactivation of I_{KIF} is crucial in determining firing pattern, a perturbation analysis was performed. Figure 9*C* illustrates the effect of perturbations of h_F from the resting value of 0.012 to values between 0.1 and 0.3 coincident with the onset of depolarization (no hyperpolarization is applied in these simulations). Figure 9*D* shows the resulting FSL (filled circles) and FISl (open triangles) for the different values of h_F . The unfilled circles correspond to the voltage traces in Fig. 9*C*. Increasing h_F from 0.1 up to 0.21 resulted in a small increase in FSL. At a value of h_F of 0.22 (vertical dashed line), a large increase in FSL was seen (arrow), which coincided with a decreased FISl. The large changes in FSL observed with a small increase in h_F to 22% are suggestive of a bifurcation. However, only a mathematical analysis of the equilibrium points of the system can definitively demonstrate a bifurcation. Nonetheless these results indicate that the critical

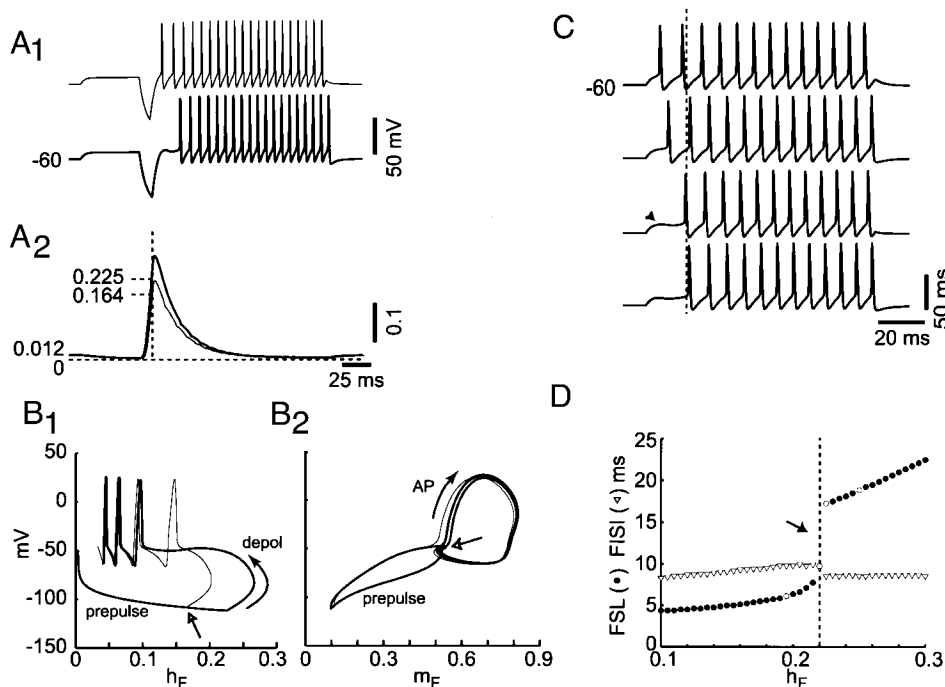


FIG. 9. Phaseplane analysis of h_F . *A1*: voltage traces with prepulses of 9.2 ms (thin line) and 10.8 ms (thick line). *A2*: h_F for the 2 traces in *A1*. Note that h_F is larger at the onset of the depolarization after a prepulse lasting 10.8 ms. *B1*: phaseplane of h_F . Note the divergence in the trajectories at an h_F of ~ 0.16 (open arrow). *B2*: phaseplane of m_F . Note the sag in the response (open arrow), corresponding to the onset delay. *C* and *D*: perturbation analysis of I_{KIF} at the “regular”/“buildup” bifurcation. h_F was stepped from the resting level of 0.012 to values between 0.1 and 0.3 coincident with the onset of depolarization to 100 pA. m_F at the onset of the step was 0.35 in all cases. *C*: 4 voltage traces for different values of h_F . Note the transition in discharge pattern. The dashed line indicates the first spike latency after the main transition. *D*: FSL (solid circles) and FISl (open triangles) for different values of h_F . The values of h_F for the traces in *C* are indicated by the unfilled circles. Note that there is a large increase in FSL for h_F of 0.22 (arrow and vertical dashed line).

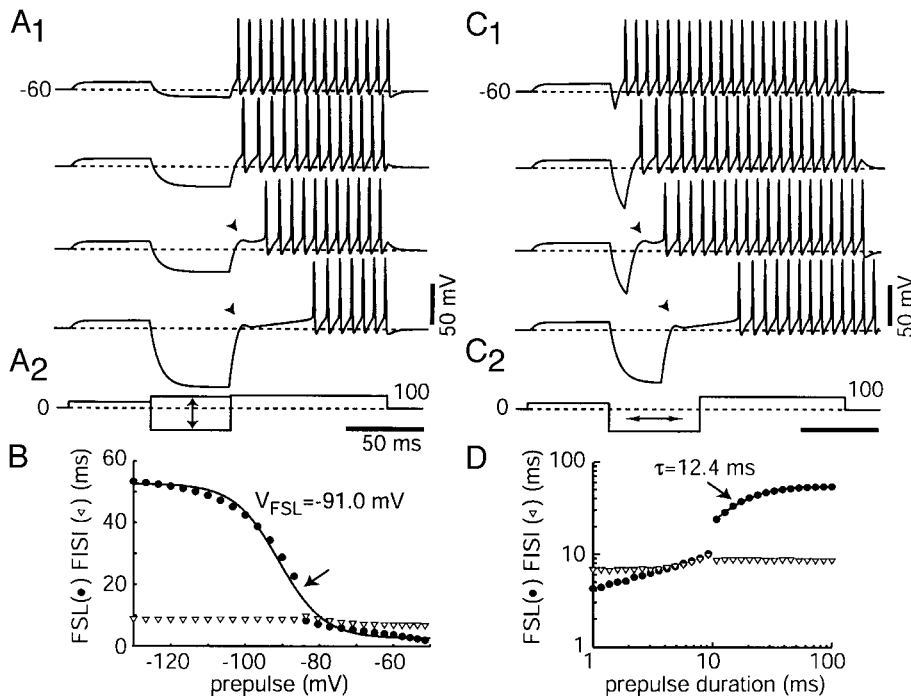


FIG. 10. Contribution of I_h to discharge patterns. *A*: effect of removing I_h on the voltage dependence of discharge patterns. *A1*: voltage traces with different prepulse amplitudes (-130.0 , -86.8 , -83.6 , and -68.0 mV). *A2*: current protocol for *A1*. *B*: dependence of the FSL (circles) and FISI (triangles) on prepulse amplitude. Compare to Fig. 3*B1*. *C*: effect of removing I_h on time dependence. *C1*: voltage traces with different prepulse durations (3.0, 9.2, 10.8, and 32.9 ms). Note the emergence of the “hump and sag” responses (arrowhead). *C2*: current protocol for *C1*. *D*: dependence of the FSL (circles) and FISI (triangles) on prepulse durations. Compare to Fig. 4*B1*.

time at which the cell shifts into a long latency firing mode is determined by the amount of I_{KIF} available at the moment of depolarization, i.e., by the amount of inactivation that has been removed during the hyperpolarization.

Influence of I_h

I_h had been included in the model to provide a substrate for the observed differences in membrane charging time constants to hyperpolarizing and depolarizing steps and to account for the observed sag in the response to hyperpolarized pulses. So far the influence of I_h on the discharge patterns was unclear. Therefore I_h was removed from the model and the voltage and time dependence of the discharge patterns were investigated. Since I_h is partially available at rest, it was necessary to adjust the leak conductance g_L to 3 nS to keep the input resistance at rest the same as in all prior simulations.

Figure 10*A* shows the discharge patterns with different prepulse amplitudes. Increasing the amount of hyperpolarization increased the FSL. The model showed a firing pattern transition between -83.6 and -86.8 mV (Fig. 10*A1*). The increase in FSL with prepulse amplitude was fitted with a Boltzmann function with a half-voltage of -91.0 mV (Fig. 10*B*). Thus the removal of I_h shifted the voltage dependence of the transition by about -2 mV (compare with Fig. 3). The retention of the hump and sag at the onset of the depolarizing step suggests that the hump and sag is not due to slow deactivation of I_h .

Lengthening the prepulse increased the FSL (Fig. 10*C*). The sharp transition between discharge pattern occurred between prepulses of 9.2 and 10.8 ms (Fig. 10*C1*), visible as steep increase in latency with increasing prepulse duration (Fig. 10*D*). The prepulse duration at which the discharge pattern transition occurs is unchanged (compare with Fig. 4). However, the recovery time constant was slightly increased to 12.4 ms (Fig. 10*D*, —).

Together these results suggest that although I_h is not respon-

sible for discharge pattern transitions, it can modulate the bifurcation-generating mechanism since its activation during hyperpolarizing steps both decreases the membrane time constant and reduces the hyperpolarization. Thus cells with a larger amount of I_h are likely to show discharge pattern transitions with smaller hyperpolarizations and at shorter prepulse duration. However, during long hyperpolarized steps, I_h causes a reduction in hyperpolarization and a decrease in the membrane time constant. Under these conditions, pauser responses are seen with depolarizations that would yield buildup responses without I_h . For example, the reduction in FSL for long prepulses in Fig. 7*C* is not present when I_h is removed (not shown).

Influence on action potential shape

One hallmark of the activity of I_{KI} in other systems is the narrowing of action potentials following hyperpolarizations or action potential widening after firing of successive action potentials (Gean and Shinnick-Gallagher 1989; Ma and Koester 1995, 1996). Therefore the effects of hyperpolarized prepulses on the shape of the *first* action potential in the pauser pattern were investigated.

Four parameters of the *first* action potential during a depolarization were characterized. The first two parameters are the maximum rising and falling slope of the spike, whereas the second two parameters are the rising and falling action potential half-widths. Figure 11 shows the four parameters as a function of prepulse voltage, comparing the control condition (●) and the effect of the removal of I_{KIF} (▽) on these four parameters. Under control conditions, the maximum rising slope of the first spike is reduced from control for prepulses negative to rest (Fig. 11*A*), indicating slowed charging of the membrane. The decrease in rising slope saturated at about -110 mV. The maximum falling slope increased for more hyperpolarized prepulses (Fig. 11*B*), indicating faster repolar-

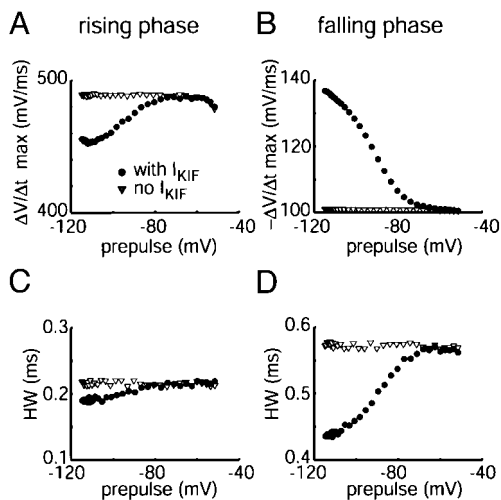


FIG. 11. Influence of I_{KIF} on 4 measures of action potential (AP) shape, as a function of prepulse voltage for the protocol shown in Fig. 3. *A*: I_{KIF} slows the rising phase of the first AP for voltages below -80 mV. The voltage-dependent effect is absent when I_{KIF} is removed. *B*: I_{KIF} speeds the falling phase (repolarization) of the 1st AP for voltages below about -80 mV. This effect is absent when I_{KIF} is removed. *C*: I_{KIF} slightly shortens the half-width of the rising phase of the action potential. This effect is absent when I_{KIF} is removed. *D*: I_{KIF} shortens the falling half-width of the action potential. This effect is absent when I_{KIF} is removed. Note that removal of I_{KIF} did not affect the shape of the AP after depolarizations from rest.

ization. The rising half-width was only slightly reduced by hyperpolarized prepulses (Fig. 11C), whereas the falling action potential half-width was strongly reduced in the presence of hyperpolarizing prepulses (Fig. 11D), consistent with a faster repolarization. The total action potential width was reduced from 0.78 to 0.63 ms at -115 mV, a decrease of $\sim 20\%$. Hyperpolarizations to -80 mV, which is in the range reached by inhibitory postsynaptic potentials (IPSPs), reduced the width of the action potential by $\sim 4\%$. Removal of I_{KIF} abolished the effects of the hyperpolarizing prepulse (Fig. 11, ∇). Removal of I_{KIF} did not alter spike shape after depolarizations from rest, which is expected because at rest most I_{KIF} is inactivated. From Fig. 11, it is evident that I_{KIF} affects the repolarization phase more strongly than the depolarization phase. These simulations demonstrate that small excursions of the membrane potential from rest before a depolarization can modify action potential shape if I_{KIF} is present in a cell.

DISCUSSION

This model captures the different discharge patterns of DCN pyramidal cells observed *in vitro* as well as the sharp, stimulus dependent transitions between the patterns. Similar to the experimentally observed behavior, the model shows that a single cell, depending on the pattern of hyperpolarization and depolarization, can generate all three patterns. Furthermore the model demonstrates that modifying the voltage- and time-dependent behavior of a single conductance can play a critical role in generating diversity in the discharge patterns.

Previous models

Previous computational models of DCN pyramidal cells using generic channel parameters (Hewitt and Meddis 1995; Kim et al. 1994; Zhao 1993) replicated some response charac-

teristics of DCN pyramidal cells, supporting the hypothesis that a transient potassium conductance could explain the different discharge patterns (Manis 1990). However, they required ad hoc, although experimentally informed, assumptions about the voltage and time dependence of the underlying ion channels. In each of these models, the absolute density of different conductances and the ratios between the magnitudes of the conductances appear to be far from experimentally observed values. In contrast to the previous models, the model presented in this paper is based on detailed physiological data and consequently should more accurately represent actual cellular dynamics. This model reproduced several salient behaviors of DCN pyramidal cells and showed clearly the intimate association of I_{KIF} and the discharge patterns. The model also predicts how modulation of I_{KIF} should affect discharge patterns.

One issue that arises is whether I_{KIF} can be sufficiently de-inactivated under normal conditions to lead to the discharge pattern changes we have modeled here. The simulation results shown seem to suggest that rather large hyperpolarizations are necessary to remove inactivation of I_{KIF} . In all of the simulations shown here, a small subthreshold depolarizing pulse was delivered prior to hyperpolarization. This pulse itself inactivates I_{KIF} and shifts the voltage dependence of the discharge patterns in a hyperpolarizing direction. We specifically used this protocol to simulate the experimental situation employed previously (Kanold and Manis 1999b). However, we have found that IPSPs evoked by parallel fiber stimulation are sufficient to move the cells from one discharge mode to another (Kanold and Manis 1999a) and that inactivation is further removed by short trains of IPSPs. Simulations with this model without the depolarizing step further support the increased availability of I_{KIF} near the resting potential.

Evidence that I_{KIF} is responsible for discharge pattern changes

Removal of I_{KIF} abolishes the dependence of the FSL shift on the presence of hyperpolarizing prepulses, providing strong evidence that I_{KIF} is responsible for the discharge pattern changes. The voltage-dependent behavior is very robust with respect to the kinetics of I_{KIF} and does not depend on a singular point in the parameter space. As such, these discharge patterns are a general consequence of the presence of I_{KIF} in a neuron. An additional membrane mechanism that might be involved in generating these discharge patterns is I_h . However, removing I_h resulted in a relatively modest change in the behavior of the model, suggesting that this conductance likely plays only a modulatory role in regulating discharge patterns.

The model suggests that the sharp discharge pattern transitions seen experimentally are caused by the availability of a critical amount of outward current carried by I_{KIF} that can oppose the inward current at depolarization onset. The underlying mechanism of the transition (the availability of I_{KIF}) is a continuous process, whereas the presence of a spike in the response is a discrete event. The hump and sag response seen at the onset of the buildup pattern is partially a remnant of the absent onset spike (caused by initial activation of Na^+ currents) and partially mediated by delayed activation of I_{KIF} and I_{KIS} . If I_{KIF} and I_{KIS} activate more rapidly, then the hump and sag are absent. Experimentally, a strong hump and sag is

frequently seen, which might be due to rapid membrane charging or to a larger amount of available I_{KIF} at rest. It should be noted that the passive membrane time constants used in the model are on the lower end of the experimentally observed range. Thus it is also possible that an additional inward current (e.g., carried by sodium or calcium ions) is involved in this behavior in pyramidal cells.

Regulation of discharge patterns by I_{KIF}

The inactivation kinetics of I_{KIF} employed in this model were based on means from experimental measurements. The voltage dependence of the FSL in the model matched the mean of the experimentally observed results for buildup cells. However, our experimental measurements revealed a range of kinetics (Kanold and Manis 1999b), which in turn could correspond to a range of firing behaviors. Some cells could easily fire in all three patterns, whereas others fired preferentially in a pauser or buildup modes (unpublished observations). The simulations show that variation of the half-inactivation of I_{KIF} (V_{KIF}) can change the half-voltage of the FSL shift, spanning the experimentally observed range. The half-voltage of the FISI shift for the pauser pattern is always negative to the half-voltage for the buildup pattern; this matches our experimental results. V_{KIF} and the half-voltage of the FSL shift show a strong correlation, whereas the dependence of the FISI in the pauser mode on channel kinetics is somewhat more complex.

The fact that the model showed all types of responses with parameter variations within the physiological range suggests that regulation of I_{KIF} might account for the variations in the observed discharge patterns. For example, the model generated pauser responses when depolarized from slightly below rest but only when V_{KIF} was shifted toward positive values. Pauser responses differ from buildup responses in the occurrence of an onset spike before the outward currents turn on. Using stronger depolarization with prepulse levels that generate buildup responses can elicit pauser responses under some conditions. Similarly, the FSL in the buildup response depends on the interaction between the channel kinetics and the hyperpolarizing inputs. The stimulus space boundary for generating a pause (long FISI) or transitioning to a long FSL can be shifted by adjusting V_{KIF} or τ_{mF}/τ_{hF} and thus the availability and rate of activation of I_{KIF} at the onset of depolarization. Evidently by adjusting these parameters, a neuron can change the relationship between the discharge pattern and stimulus conditions.

There is emerging evidence that individual neurons may adjust the operating points of their ion channels in response to their activity or the activity of their afferents (Aizenman and Linden 2000; Desai et al. 1999; Golowasch et al. 1999; LeMasson et al. 1993; Stemmler and Koch 1999; Turrigiano et al. 1996). This is an important concept since it potentially adds to the diversity and dynamics of information processing mechanisms available to neurons. Although the most commonly considered feedback mechanism is intracellular calcium, sensing the spiking activity of the cell over various time scale(s) (Liu et al. 1998; Shin et al. 1999), other mechanisms undoubtedly exist. If cells adjust their channel expression or channel function, then the intrinsic discharge patterns of a cell may be quantitatively unique depending on the cell's stimulus and activity history (Jaeger and Bower

1999); individual cells may be "tuned" to have increased or decreased sensitivity to particular regimes of spatiotemporal patterns of synaptic input.

We previously postulated that rapidly inactivating I_{KIF} currents in the DCN arise from channels composed of $K_v4.2$ and possibly $K_v4.3$, based on both kinetics and pharmacology (Kanold and Manis 1999b). $K_v4.2$ specifically is highly expressed in the cochlear nucleus, including in pyramidal cells (Fitzakerley et al. 2000). The K_v4 family of channels has been shown to associate with a family of potassium-channel interacting proteins (KChIP) (An et al. 2000). These proteins contain four E-F hand domains that bind calcium and that ultimately impart a calcium regulation of the channels. When associated with K_v4 channels, KChIP subunits can modulate inactivation time constants and the rate of recovery from inactivation as well as the activation voltage dependence. Thus in principle, calcium acting through an auxiliary subunit is one way to modulate these channels. $K_v4.2$ channels can also be modulated by protein kinase C (PKC), several isoforms of which are abundant in DCN neurons, including pyramidal cells (Garcia and Harlan 1997; Garcia et al. 1993; Saito et al. 1988). The effect of PKC activation is a rapidly developing, dose-dependent and pharmacologically specific decrease in the total outward current through $K_v4.2$ channels without any effect on the voltage or time dependence of the current in expression systems (Nakamura et al. 1997) and with a modest reduction of the availability of the conductance in intact systems (Hoffman and Johnston 1998). cAMP-dependent protein kinase (PKA) can likewise phosphorylate $K_v4.2$ (Anderson et al. 2000) and has effects similar to PKC on native channels (Hoffman and Johnston 1998), decreasing total available current at a given voltage. Both PKC and PKA can shift the voltage dependence of inactivation ≤ 8 mV. However, the effects of PKC and PKA on the inactivation rates are not as large as those produced by association with Ca^{2+} -bound KChIP, suggesting that channel availability and kinetics may be modulated somewhat independently. Together, these results raise the likely possibility that $K_v4.2$ and/or $K_v4.3$ are targets of modulation by either calcium or protein kinases in pyramidal cells.

Another implication of our modeling results is that a morphologically defined class of cells can show diverse discharge patterns due to differences in the specific properties of intrinsic conductances. Since the specific functional properties in part depend on posttranslational modifications of the ion channels (as discussed in the preceding text), it follows that the discharge patterns may not be strictly correlated with the overall pattern of ion channel expression. Consequently the association of a particular discharge pattern observed in vivo with a particular cell type, as is sometimes assumed to be the case, becomes somewhat problematic as noted previously in the cochlear nucleus (Ding et al. 1999; Rhode et al. 1983; Rouiller and Ryugo 1984). Ultimately identical patterns of excitatory and inhibitory input may generate a characteristic response in each cell that depends on the cells history and function. However, the possible repertoire of discharge patterns that can be generated will be limited by the specific types of channels expressed in a cell and their spatial pattern of insertion in the cell membrane.

Changes in action potential shape

The presence of I_{KIF} in the cell reduced the duration of the first action potential following hyperpolarizing prepulses. This is similar to results in rat amygdala neurons where I_{KI} causes a narrowing of the first action potential following a depolarization from a hyperpolarized potential by 14% (Gean and Shinnick-Gallagher 1989). Action potential widening can lead to increased Ca^{2+} influx; this, in terminals, leads to altered neurotransmitter release (Augustine 1990; Bourque 1991; Coates and Bulloch 1985; Eliot et al. 1993; Giese et al. 1998; Gillette et al. 1980; Jackson et al. 1991; Lin and Faber 1988; Mudge et al. 1979). At the squid giant synapse, a 30% increase in presynaptic action potential width increased total presynaptic calcium influx by 230% (Augustine 1990). Therefore depending on the specific set of Ca^{2+} conductances, it is possible that action potential narrowing due to preceding hyperpolarization (i.e., IPSPs) can cause a significant decrease in Ca^{2+} influx for backpropagating action potentials, which are present in pyramidal cells (Manis and Molitor 1996).

Ca^{2+} influx via backpropagating action potentials can lead to altered cellular excitability (Aizenman and Linden 2000) or changes in synaptic strength (Markram et al. 1997). Hence modulation of the first action potential in the response may affect its ability to induce such changes, e.g., for brief stimuli. Recent studies showed impaired associative memory and learning after removal of K^+ channels and that this effect might be due to altered Ca^{2+} influx caused by spike broadening (Giese et al. 1998; Meiri et al. 1997). Thus the presence of I_{KIF} in DCN pyramidal cells can potentially influence the synaptic and integrative properties of these cells following hyperpolarization and might ultimately contribute to other short- and long-term changes in cell function.

Functional implications

The pyramidal cells receive inhibitory input from at least three distinct sources. A significant source of hyperpolarization is inhibitory input from DCN cartwheel cells (Davis and Young 1997; Davis et al. 1996; Zhang and Oertel 1994) that is of relatively long duration (10–30 ms). Input to the cartwheel cells arises from parallel fibers that carry both auditory and nonauditory input [e.g., somatosensory input from the pinna (Kanold and Young 1998; Young et al. 1995)]. If hyperpolarization from these cells deinactivates I_{KIF} , then I_{KIF} may play an important role in the integration of auditory and nonauditory information as it allows prior nonauditory input to modify the acoustically evoked response. Consequently the response of DCN pyramidal cells to auditory stimuli can be highly dependent on nonauditory context. Another important inhibitory input arises from the vertical or tuberculoventral cells (Brawer et al. 1974; Lorente de No 1933; Rhode 1999; Zhang and Oertel 1993), which are thought to play a critical role in the generation of the acoustic responses of the pyramidal cells. Based on the interpretation of cross-correlation analyses (Voigt and Young 1980) and current-source density analysis (Manis and Brownell 1983), these cells presumably provide brief IPSPs to the pyramidal cells. Presumably individual IPSPs from these cells would be less effective than the slow cartwheel cell IPSPs in deinactivating I_{KIF} because of their brief time course, but this could be overcome by summation over time

and by convergence. A third source of inhibition is the wide-band inhibitory input. This input is necessary to explain the response maps of pyramidal and vertical cells (Davis and Young 2000; Nelken and Young 1994; Spirou and Young 1991; Spirou et al. 1999) and is postulated to arise from the onset-C cells of the VCN (Doucet and Ryugo 1997; Jiang et al. 1996; Smith and Rhode 1989). The temporal properties of inhibition produced by this input are not known. In principle, either of these latter inputs could effectively utilize I_{KIF} to alter the firing patterns of pyramidal cells depending on the spectro-temporal structure of the acoustic input (for example, see Palombi et al. 1994; Parham and Kim 1993).

The dependence of the discharge pattern on the historical combination of hyperpolarization and depolarization as reflected in the inactivation and activation of I_{KIF} suggests a simple mechanism of encoding temporal information by a population of cells. Cells expressing I_{KIF} with different inactivation characteristics, yet receiving identical patterns of synaptic input, would respond to a common temporal sequence of activity with different firing patterns. Across a population of such cells, the driving activity will be encoded in the relative latencies and interspike intervals. This timing, as regulated by I_{KIF} , would then carry a code for the recent history of activity in inhibitory, as well as excitatory, inputs to the cell.

We thank E. D. Young and D. O. Kim for insightful discussions during this project.

This work was supported by National Institute on Deafness and Other Communication Disorders Grant R01 DC-00425 to P. B. Manis.

Present address of P. O. Kanold: Harvard Medical School, Dept. of Neurobiology, Goldenson Bldg. 405, 220 Longwood Ave., Boston, MA 02115.

REFERENCES

- AIZENMAN CD AND LINDEN DJ. Rapid, synaptically driven increases in the intrinsic excitability of cerebellar deep nuclear neurons. *Nat Neurosci* 3: 109–111, 2000.
- AN WF, BOWLBY MR, BETTY M, CAO J, LING HP, MENDOZA G, HINSON JW, MATSSON KI, STRASSLE BW, TRIMMER JS, AND RHODES KJ. Modulation of A-type potassium channels by a family of calcium sensors. *Nature* 403: 553–556, 2000.
- ANDERSON AE, ADAMS JP, QIAN Y, COOK RG, PFAFFINGER PJ, AND SWEATT JD. Kv4.2 phosphorylation by cyclic AMP-dependent protein kinase. *J Biol Chem* 275: 5337–5346, 2000.
- AUGUSTINE GJ. Regulation of transmitter release at the squid giant synapse by presynaptic delayed rectifier potassium current. *J Physiol (Lond)* 431: 343–364, 1990.
- BERNANDER O, KOCH C, AND DOUGLAS RJ. Amplification and linearization of distal synaptic input to cortical pyramidal cells. *J Neurophysiol* 72: 2743–2753, 1994.
- BOURQUE CW. Activity-dependent modulation of nerve terminal excitation in a mammalian peptidergic system. *Trends Neurosci* 14: 28–30, 1991.
- BRAWER JR, MOREST DK, AND KANE EC. The neuronal architecture of the cochlear nucleus of the cat. *J Comp Neurol* 155: 251–300, 1974.
- COATES CJ AND BULLOCH AG. Synaptic plasticity in the molluscan peripheral nervous system: physiology and role for peptides. *J Neurosci* 5: 2677–2684, 1985.
- COLBERT CM AND JOHNSTON D. Axonal action-potential initiation and Na^+ channel densities in the soma and axon initial segment of subicular pyramidal neurons. *J Neurosci* 16: 6676–6686, 1996.
- CONNOR JA AND STEVENS CF. Voltage clamp studies of a transient outward membrane current in gastropod neural somata. *J Physiol (Lond)* 213: 21–30, 1971.
- CONNOR JA, WALTER D, AND MCKOWN R. Neural repetitive firing: modifications of the Hodgkin-Huxley axon suggested by experimental results from crustacean axons. *Biophys J* 18: 81–102, 1977.
- DAVIS KA, MILLER RL, AND YOUNG ED. Effects of somatosensory and parallel-fiber stimulation on neurons in dorsal cochlear nucleus. *J Neurophysiol* 76: 3012–3024, 1996.

- DAVIS KA AND YOUNG ED. Granule cell activation of complex-spiking neurons in dorsal cochlear nucleus. *J Neurosci* 17: 6798–6806, 1997.
- DAVIS KA AND YOUNG ED. Pharmacological evidence of inhibitory and disinhibitory neuronal circuits in dorsal cochlear nucleus. *J Neurophysiol* 83: 926–940, 2000.
- DESAI NS, RUTHERFORD LC, AND TURRIGIANO GG. Plasticity in the intrinsic excitability of cortical pyramidal neurons. *Nat Neurosci* 2: 515–520, 1999.
- DESTEXHE A AND BABLOYANTZ A. A model of the inward current I_h and its possible role in thalamocortical oscillations. *Neuroreport* 4: 223–226, 1993.
- DESTEXHE A, BABLOYANTZ A, AND SEJNOWSKI TJ. Ionic mechanisms for intrinsic slow oscillations in thalamic relay neurons. *Biophys J* 65: 1538–1552, 1993.
- DING J, BENSON TE, AND VOIGT HF. Acoustic and current-pulse responses of identified neurons in the dorsal cochlear nucleus of unanesthetized, decerebrate gerbils. *J Neurophysiol* 82: 3434–3457, 1999.
- DOUCET JR AND RYUGO DK. Projections from the ventral cochlear nucleus to the dorsal cochlear nucleus in rats. *J Comp Neurol* 385: 245–264, 1997.
- ELIOT LS, KANDEL ER, SIEGELBAUM SA, AND BLUMENFELD H. Imaging terminals of Aplysia sensory neurons demonstrates role of enhanced Ca^{2+} influx in presynaptic facilitation. *Nature* 361: 634–637, 1993.
- FITZAKERLEY JL, STAR KV, RINN JL, AND ELMQUIST BJ. Expression of shal potassium channel subunits in the adult and developing cochlear nucleus of the mouse. *Hear Res* 147: 31–45, 2000.
- GARCIA MM, CUSICK CG, AND HARLAN RE. Protein kinase C-delta in rat brain: association with sensory neuronal hierarchies. *J Comp Neurol* 331: 375–388, 1993.
- GARCIA MM AND HARLAN RE. Protein kinase C in central auditory pathways of the rat. *J Comp Neurol* 385: 1–25, 1997.
- GEAN PW AND SHINNICK-GALLAGHER P. The transient potassium current, the A-current, is involved in spike frequency adaptation in rat amygdala neurons. *Brain Res* 480: 160–169, 1989.
- GEISE KP, STORM JF, REUTER D, FEDOROV NB, SHAO LR, LEICHER T, PONGS O, AND SILVA AJ. Reduced K⁺ channel inactivation, spike broadening, and after-hyperpolarization in Kv β 1.1-deficient mice with impaired learning. *Learn Mem* 5: 257–273, 1998.
- GILLETTE R, GILLETTE MU, AND DAVIS WJ. Action-potential broadening and endogenously sustained bursting are substrates of command ability in a feeding neuron of Pleurobranchaea. *J Neurophysiol* 43: 669–685, 1980.
- GODFREY DA, KIANG NY, AND NORRIS BE. Single unit activity in the dorsal cochlear nucleus of the cat. *J Comp Neurol* 162: 269–284, 1975.
- GOLOWASCH J, ABBOTT LF, AND MARDER E. Activity-dependent regulation of potassium currents in an identified neuron of the stomatogastric ganglion of the crab *Cancer borealis*. *J Neurosci* 19: RC33, 1999.
- HEWITT MJ AND MEDDIS R. A computer model of dorsal cochlear nucleus pyramidal cells: intrinsic membrane properties. *J Acoust Soc Am* 97: 2405–2413, 1995.
- HILLE B. *Ionic Channels of Excitable Membranes*. Sunderland, MA: Sinauer, 1992.
- HINES ML AND CARNEVALE NT. The NEURON simulation environment. *Neural Comput* 9: 1179–1209, 1997.
- HIRSCH JA AND OERTEL D. Intrinsic properties of neurons in the dorsal cochlear nucleus of mice, in vitro. *J Physiol (Lond)* 396: 535–548, 1988.
- HODGKIN AL AND HUXLEY AF. A quantitative description of membrane current and its application to conduction and excitation in nerve. *J Physiol (Lond)* 117: 500–544, 1952.
- HOFFMAN DA AND JOHNSTON D. Downregulation of transient K⁺ channels in dendrites of hippocampal CA1 pyramidal neurons by activation of PKA and PKC. *J Neurosci* 18: 3521–3528, 1998.
- JACKSON MB, KONNERTH A, AND AUGUSTINE GJ. Action potential broadening and frequency-dependent facilitation of calcium signals in pituitary nerve terminals. *Proc Natl Acad Sci USA* 88: 380–384, 1991.
- JAEGER D AND BOWER JM. Synaptic control of spiking in cerebellar Purkinje cells: dynamic current clamp based on model conductances. *J Neurosci* 19: 6090–6101, 1999.
- JIANG D, PALMER AR, AND WINTER IM. Frequency extent of two-tone facilitation in onset units in the ventral cochlear nucleus. *J Neurophysiol* 75: 380–395, 1996.
- KANOLD PO AND MANIS PB. Non-coincident inhibition modifies the discharge patterns of pyramidal cells in the dorsal cochlear nucleus. *Soc Neurosci Abstr* 25: 397, 1999a.
- KANOLD PO AND MANIS PB. Transient potassium currents regulate the discharge patterns of dorsal cochlear nucleus pyramidal cells. *J Neurosci* 19: 2195–2208, 1999b.
- KANOLD PO AND YOUNG ED. Somatosensory input to the cat dorsal cochlear nucleus (DCN) derives primarily from spinal nerve C2. *Assoc Res Otolaryngol* 21: 98, 1998.
- KIM DO, GHOSHAL S, KHANT SL, AND PARHAM K. A computational model with ionic conductances for the fusiform cell of the dorsal cochlear nucleus. *J Acoust Soc Am* 96: 1501–1514, 1994.
- LEMASSEON G, MARDER E, AND ABBOTT LF. Activity-dependent regulation of conductances in model neurons. *Science* 259: 1915–1917, 1993.
- LIN JW AND FABER DS. Synaptic transmission mediated by single club endings on the goldfish Mauthner cell. II. Plasticity of excitatory postsynaptic potentials. *J Neurosci* 8: 1313–1325, 1988.
- LIU Z, GOLOWASCH J, MARDER E, AND ABBOTT LF. A model neuron with activity-dependent conductances regulated by multiple calcium sensors. *J Neurosci* 18: 2309–2320, 1998.
- LLINAS RR. The intrinsic electrophysiological properties of mammalian neurons: insights into central nervous system function. *Science* 242: 1654–1664, 1988.
- LORENTE DE NO R. Anatomy of the eighth nerve. III. General plan of structure of the primary cochlear nuclei. *Laryngoscope* 43: 327–350, 1933.
- MA M AND KOESTER J. Consequences and mechanisms of spike broadening of R20 cells in Aplysia californica. *J Neurosci* 15: 6720–6734, 1995.
- MA M AND KOESTER J. The role of K⁺ currents in frequency-dependent spike broadening in Aplysia R20 neurons: a dynamic-clamp analysis. *J Neurosci* 16: 4089–4101, 1996.
- MANIS PB. Membrane properties and discharge characteristics of guinea pig dorsal cochlear nucleus neurons studied in vitro. *J Neurosci* 10: 2338–2351, 1990.
- MANIS PB AND BROWNELL WE. Synaptic organization of eighth nerve afferents to cat dorsal cochlear nucleus. *J Neurophysiol* 50: 1156–1181, 1983.
- MANIS PB AND MOLITOR SC. Evoked calcium transients in dendrites of rat dorsal cochlear nucleus neurons. *Abstr Assoc Res Otolaryngol* 19: 169, 1996.
- MARKRAM H, LUBKE J, FROTSCHER M, AND SAKMANN B. Regulation of synaptic efficacy by coincidence of postsynaptic APs and EPSPs. *Science* 275: 213–215, 1997.
- MEIRI N, GHELARDINI C, TESCO G, GALEOTTI N, DAHL D, TOMSIC D, CAVALLARO S, QUATTRONE A, CAPACCIOLI S, BARTOLINI A, AND ALKON DL. Reversible antisense inhibition of Shaker-like Kv1.1 potassium channel expression impairs associative memory in mouse and rat. *Proc Natl Acad Sci USA* 94: 4430–4434, 1997.
- MOLITOR SC AND MANIS PB. Calcium signaling in dendrites of dorsal cochlear nucleus neurons. *Soc Neurosci Abstr* 22: 647, 1996.
- MOORE JW AND COX EB. A kinetic model for the sodium conductance system in squid axon. *Biophys J* 16: 171–192, 1976.
- MUDGE AW, LEEMAN SE, AND FISCHBACH GD. Enkephalin inhibits release of substance P from sensory neurons in culture and decreases action potential duration. *Proc Natl Acad Sci USA* 76: 526–530, 1979.
- NAKAMURA TY, COETZEE WA, VEGA-SAENZ DE MIERA E, ARTMAN M, AND RUDY B. Modulation of Kv4 channels, key components of rat ventricular transient outward K⁺ current, by PKC. *Am J Physiol Heart Circ Physiol* 273: H1775–H1786, 1997.
- NELKEN I AND YOUNG ED. Two separate inhibitory mechanisms shape the responses of dorsal cochlear nucleus type IV units to narrowband and wideband stimuli. *J Neurophysiol* 71: 2446–2462, 1994.
- PALOMBI PS, BACKOFF PM, AND CASPARY DM. Paired tone facilitation in dorsal cochlear nucleus neurons: a short-term potentiation model testable in vivo. *Hear Res* 75: 175–183, 1994.
- PARHAM K AND KIM DO. Discharge suppression in the silent interval preceding the tone burst in pause-build units of the dorsal cochlear nucleus of the unanesthetized decerebrate cat. *J Acoust Soc Am* 94: 3227–3231, 1993.
- PFEIFFER RR. Classification of response patterns of spike discharges for units in the cochlear nucleus: tone-burst stimulation. *Exp Brain Res* 1: 220–235, 1966.
- RHODE WS. Vertical cell responses to sound in cat dorsal cochlear nucleus. *J Neurophysiol* 82: 1019–1032, 1999.
- RHODE WS, SMITH PH, AND OERTEL D. Physiological response properties of cells labeled intracellularly with horseradish peroxidase in cat dorsal cochlear nucleus. *J Comp Neurol* 213: 426–447, 1983.
- ROULLER EM AND RYUGO DK. Intracellular marking of physiologically characterized cells in the ventral cochlear nucleus of the cat. *J Comp Neurol* 225: 167–186, 1984.

- SAITO N, KIKKAWA U, NISHIZUKA Y, AND TANAKA C. Distribution of protein kinase C-like immunoreactive neurons in rat brain. *J Neurosci* 8: 369–382, 1988.
- SHIN J, KOCH C, AND DOUGLAS R. Adaptive neural coding dependent on the time-varying statistics of the somatic input current. *Neural Comput* 11: 1893–1913, 1999.
- SMITH PH AND RHODE WS. Structural and functional properties distinguish two types of multipolar cells in the ventral cochlear nucleus. *J Comp Neurol* 282: 595–616, 1989.
- SPIROU GA, DAVIS KA, NELKEN I, AND YOUNG ED. Spectral integration by type II interneurons in dorsal cochlear nucleus. *J Neurophysiol* 82: 648–663, 1999.
- SPIROU GA AND YOUNG ED. Organization of dorsal cochlear nucleus type IV unit response maps and their relationship to activation by bandlimited noise. *J Neurophysiol* 66: 1750–1768, 1991.
- STEMMLER M AND KOCH C. How voltage-dependent conductances can adapt to maximize the information encoded by neuronal firing rate. *Nat Neurosci* 2: 521–527, 1999.
- STUART G, SPRUSTON N, SAKMANN B, AND HAUSSER M. Action potential initiation and backpropagation in neurons of the mammalian CNS. *Trends Neurosci* 20: 125–131, 1997.
- TURRIGIANO GG, MARDER E, AND ABBOTT LF. Cellular short-term memory from a slow potassium conductance. *J Neurophysiol* 75: 963–966, 1996.
- VOIGT HF AND YOUNG ED. Evidence of inhibitory interactions between neurons in dorsal cochlear nucleus. *J Neurophysiol* 44: 76–96, 1980.
- YOUNG ED, NELKEN I, AND CONLEY RA. Somatosensory effects on neurons in dorsal cochlear nucleus. *J Neurophysiol* 73: 743–765, 1995.
- ZHANG S AND OERTEL D. Tuberculoventral cells of the dorsal cochlear nucleus of mice: intracellular recordings in slices. *J Neurophysiol* 69: 1409–1421, 1993.
- ZHANG S AND OERTEL D. Neuronal circuits associated with the output of the dorsal cochlear nucleus through fusiform cells. *J Neurophysiol* 71: 914–930, 1994.
- ZHAO Z. *A Physiological Model of DCN Fusiform Cell In Vitro Studies* (MSc thesis). Baltimore, MD: Johns Hopkins University, 1993.